# Highly Efficient Cadmium-Free Quantum Dot Light-Emitting Diodes Enabled by the Direct Formation of Excitons within InP@ZnSeS Quantum Dots

**Jaehoon Lim,[†,‡,⊥] Myeongjin Park,[‡,⊥] Wan Ki Bae,[△] Donggu Lee,[‡] Seonghoon Lee,[§,*] Changhee Lee,[‡,*] and Kookheon Char[†,*]**

[†]School of Chemical & Biological Engineering, The National Creative Research Initiative Center for Intelligent Hybrids, The WCU Program of Chemical Convergence for Energy & Environment, Seoul National University, 1 Gwanak-ro, Gwanak-gu, Seoul 151-744, Korea, [‡]Department of Electrical & Computer Engineering, Inter-University Semiconductor Research Center, Seoul National University, 1 Gwanak-ro, Gwanak-gu, Seoul 151-744, Korea, [§]School of Chemistry, Seoul National University, 1 Gwanak-ro, Gwanak-gu, Seoul 151-747, Korea, and [△]Photo-Electronic Hybrids Research Center, Korea Institute of Science and Technology, Seoul 136-791, Korea. [⊥]These authors contributed equally.

**ABSTRACT** We demonstrate bright, efficient, and environmentally benign InP quantum dot (QD)-based light-emitting diodes (QLEDs) through the direct charge carrier injection into QDs and the efficient radiative exciton recombination within QDs. The direct exciton formation within QDs is facilitated by an adoption of a solution-processed, thin conjugated polyelectrolyte layer, which reduces the electron injection barrier between cathode and QDs *via* vacuum level shift and promotes the charge carrier balance within QDs. The efficient radiative recombination of these excitons is enabled in structurally engineered InP@ZnSeS heterostructured QDs, in which excitons in the InP domain are effectively passivated by thick ZnSeS composition-gradient shells. The resulting QLEDs record 3.46% of external quantum efficiency and 3900 cd $m^{-2}$ of maximum brightness, which represent 10-fold increase in device efficiency and 5-fold increase in brightness compared with previous reports. We believe that such a comprehensive scheme in designing device architecture and the structural formulation of QDs provides a reasonable guideline for practical realization of environmentally benign, high-performance QLEDs in the future.

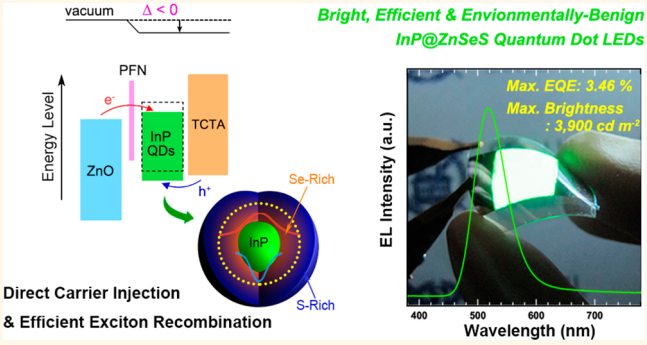


**KEYWORDS:** InP quantum dots · core@shell heterostructure · electroluminescence devices · conjugated polyelectrolyte

Colloidal quantum dot (QD)-based electroluminescent light-emitting diodes (QLEDs) have been considered as one of the future display technologies, featuring high color purity, flexibility, transparency, and cost efficiency based on low-temperature, solution-based processing methods. This ever-increasing attention stems from distinct optical properties of QDs, such as convenient band gap tunability, narrow emission bandwidth, and high photoluminescence quantum yield (PL QY), which far surpass those of conventional organic dyes or inorganic phosphors.[1] Since the first demonstration of QLEDs, multilateral efforts have been continued to exploit the excellent optical properties of QDs in the framework of an electroluminescence (EL) mechanism. Advances in synthetic chemistry enabled structural engineering of QDs into various shapes with atomic scale precision. The representative example is the synthesis of highly monodisperse, efficient, and stable core@shell heterostructured QDs with tailored photophysical properties.[2−7] In addition, deeper understanding on device operational mechanism guided the structural engineering of QLEDs to realize efficient charge carrier injection and exciton recombination in QD active layers. As a

* Address correspondence to khchar@plaza.snu.ac.kr, chlee7@snu.ac.kr, shnlee@snu.ac.kr.

Received for review July 14, 2013 and accepted September 13, 2013.

**Published online September 24, 2013**
**10.1021/nn403594j**

result of the continued innovation, QLEDs evolved to have multilayered structures with balanced charged injection into QDs with device efficiency as high as the theoretical limit.[8] Moreover, the knowledge accumulated on unit devices prompted research on new fabrication methods such as microcontact printing[9−11] or inkjet printing,[12,13] enabling successful demonstration of active matrix-driven full-color QD displays.[11,14]

Despite rapid improvement and promising outlook, the commercialization of QLEDs is strictly restricted by the use of hazardous substances in QDs (*i.e.*, Cd and Pb). Although tight encapsulation technology and recycling policy could potentially mitigate the environmental concerns, fundamental solutions are still needed to prevent the use of heavy metal elements and thus to promote the persistent development of QD-based optoelectronic devices. Among other potential replacements of Cd-based II−VI compounds, InP QDs[3,4,23−25] have been suggested as the most promising candidate for light-emitting applications due to their band gap tunability covering the entire visible range and narrow spectral bandwidth. For that reason, the preparation of high-quality InP QDs has been actively pursued in the framework of electroluminescence or down-conversion light-emitting applications.

Although ever-increasing attention to InP QDs is now leading to applied research on InP QLEDs, their full potential has not been demonstrated yet. To date, the best InP QLEDs recorded only 0.26% of EQE and 700 cd $m^{-2}$ of maximum brightness.[15] These values are indeed far inferior to QLEDs with other alternative materials with relatively lower solution PL QY, such as Si (up to 1.1% of EQE for red emission)[16] or $CuInS_2$ (up to 2100 cd $m^{-2}$ of maximum brightness for orange-red emission).[17] In addition, the color purity of previous InP QLEDs was lower than expected from solution PL spectra, deteriorated by unexpected contribution of broad parasitic emission from adjacent charge-transporting layers. Considering that InP QDs possess comparable energy levels with alternative emitting materials (valence band maximum (VBM): 3.5−4 eV and conduction band minimum (CBM): 5.5−6 eV) and they employ similar device structures, the reason for the inferior performance of InP QLEDs has still been veiled.

Herein, we demonstrate bright, efficient, and environmentally benign green-emitting InP QLEDs exhibiting EQE as high as 3.46% and brightness up to 3900 cd $m^{-2}$. This breakthrough in device performances is achieved by the device architecture for direct charge carrier injection into QDs and the structural formulation of InP@ZnSeS core@shell heterostructured QDs for efficient exciton recombination. The direct charge carrier (particularly electron) injection within QDs is assisted by a solution-processed, thin conjugated polyelectrolyte layer (poly[(9,9-bis(3′-(*N*,*N*-dimethylamino)propyl)-2,7-fluorene)-*alt*-2,7-(9,9-ioctylfluorene) (PFN)). The PFN layer essentially acts as an interfacial dipole layer between the ZnO electron transport layer and QDs, reduces the electron injection barrier into QDs through the vacuum level shift, and promotes the charge balance within QDs. On the basis of this tailored device structure, we employ highly efficient green InP QDs with thick composition-gradient ZnSeS multishells (PL QE > 70% with ∼6 monolayers of ZnSeS alloy layers). The thick ZnSeS composition-gradient multishells provide a sufficient potential barrier for the effective confinement of generated excitons within the InP core domain away from the surface defect states. As a result of the finely tuned device structure along with the protection of excitons from quenching by surface defect states, the radiative recombination of electrically generated excitons was considerably enhanced, realizing InP QLEDs with high efficiency and brightness.

## RESULTS AND DISCUSSION

We designed green-emitting InP@ZnSeS core@composition-gradient shell heterostructured QDs, in which the majority of Se resides close to the InP core domain and S dominantly locates outward of the shells.[18] The presence of high Se contents (Supporting Information Table S1, ∼55%) near the InP core alleviates the compressive lattice strain between the InP core phase and the ZnS outermost shell phase (lattice mismatch = 8.5%) and thus suppresses the formation of interfacial defects, which is responsible for the nonradiative exciton recombination process. For the uniform growth of highly crystalline ZnSeS composition-gradient shells on top of InP cores, we adopted precursors with low reactivity (*i.e.*, 1-dodecanethiol for S precursors instead of *S*-trioctylphosphine) and proceeded the shell growth at elevated reaction temperature (300 °C) to induce thermodynamic shell growth conditions. The reaction schemes involve multiple shell growth steps for the thick ZnSeS shell in order to prevent the inhomogeneous shell growth or homogeneous nucleation of ZnSeS particles under high precursor concentration.

Figure 1 represents the characteristics of prepared InP@ZnSeS QDs. We started from the same sized InP QDs with an average diameter of 1.1 nm (estimated from first excitonic transition peak) and proceeded with the multiple ZnSeS shelling with different compositions and shell thicknesses. Surprisingly, InP@ZnSeS QDs showed excellent PL QY for the optimized content of Se even with large shell thickness (see Table S1): PL QY over 80% for InP@ZnSeS QDs with 1.1 nm shell thickness (Figure 1a) and over 70% for InP@ZnSeS with 1.7 nm shell thickness (Figure 1b) in the green emission range ($\lambda_{max}$: 500−520 nm, fwhm ∼50 nm). Compared with previous InP-based QDs reporting 40−60% of PL QY only for thin ZnS[2] or ZnSe/ZnS shells (thickness below 1 nm),[5,19] such high PL QY of QDs in the present study strongly supports that the composition-gradient ZnSeS multishells effectively mitigate the lattice strain

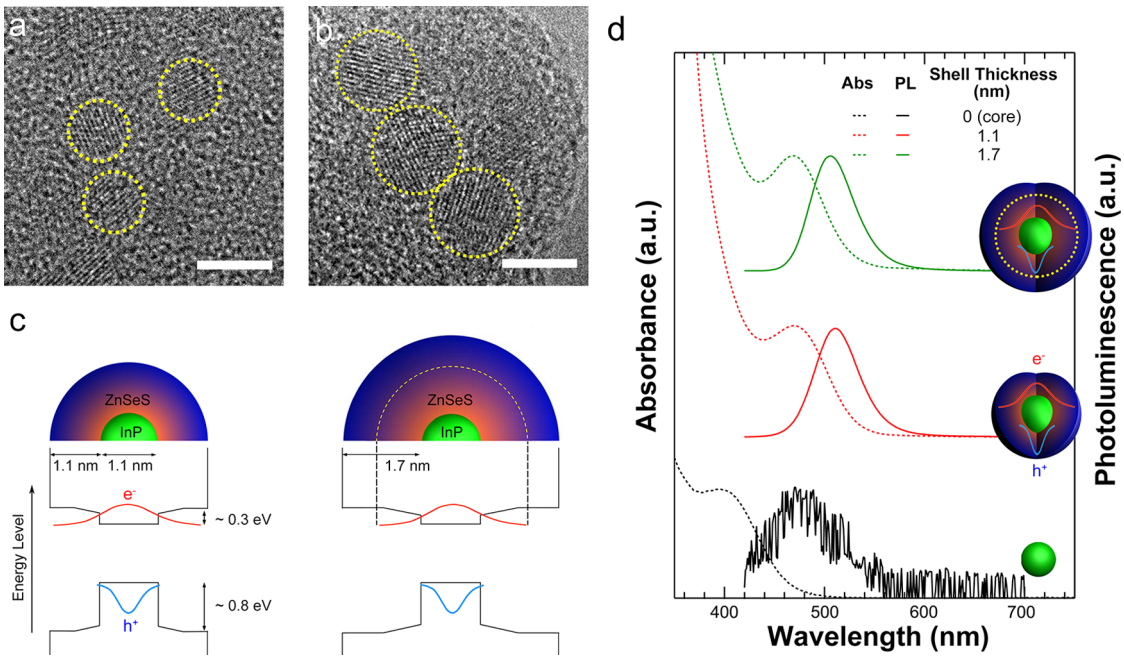


**Figure 1. High-resolution transmission electron microscopy (TEM) images of InP (diameter = 1.1 nm)@ZnSeS QDs with (a) 1.1 nm shell thickness and (b) 1.7 nm shell thickness (scale bars: 5 nm). (c) Band structure of InP@ZnSeS QDs with 1.1 nm shell thickness (left) and 1.7 nm shell thickness (right). While hole wave functions are mostly confined in the InP core phase, electron wave functions are delocalized to the shell phase (~1.1 nm shell thickness). A dashed line on the right scheme denotes a confinement region of electron wave functions. (d) Absorption (dotted lines) and photoluminescence (solid lines) spectra of InP core (black), InP@ZnSeS QDs with 1.1 nm shell thickness (red) and InP@ZnSeS QDs with 1.7 nm shell thickness (green). Schematic illustrations are included.**

even for large shell thickness. No significant changes were observed either in the PL wavelength or in the single exciton decay dynamics for a series of InP@ZnSeS QDs with different shell thicknesses, indicating that charge carrier wave functions are effectively confined within an inner shell (1.1 nm) and not affected by the additional ZnSeS shell layers. The combined consideration of the energy offset between InP core and ZnSeS shell (CBM offset ~0.3 eV, VBM offset ~0.8 eV)[18] and the effective mass of charge carriers ($m_e = 0.077$, $m_h = 0.64$ for InP) suggests that the hole is strongly confined within the InP core domain, whereas the electron is rather delocalized to the ZnSeS shell phase only to a limited extent (~1.1 nm) (Figure 1c), similar to the case of CdSe@CdS core@shell heterostructures.[20−22] Prepared InP@ZnSeS QDs recorded ~5.9 eV for VBM and ~3.5 eV for CBM, as estimated from ultraviolet photoelectron spectroscopy (UPS) and UV−visible absorption measurements (Figure S1 and Table S2). We note that the energy level positions of InP@ZnSeS QDs are closer to the vacuum level when compared with Cd-based green QDs.[23]

We adopted the inverted device structure, where a transparent ITO electrode serves as a cathode and Al as an anode (Figure 2a). The inverted device structure with hybrid (organic and inorganic) charge-transport layers is known to be particularly useful to optimize the carrier transport in QLEDs.[23] The underlying metal oxide electron transport layers (ETLs) facilitate the barrier-less injection of electrons from the cathode (ITO) and also provide mechanical robustness for the deposition of QDs based on solution-processing methods and hole-transport layers (HTL)/anode processed by vacuum evaporation or sputtering methods. In addition, the inverted device structure enables the full utilization of commercially available hole-transporting materials with proven electric property and stability. In the present study, we adopted ZnO nanoparticle thin films as ETL and 4,4′,4″-tris(*N*-carbazolyl)triphenylamine (TCTA) as the HTL. The ZnO nanoparticle thin film is highly advantageous for electroluminescence devices due to its optical transparency in the visible region (band gap ~3.3 eV) and solution processability at low temperature (<100 °C).[23] TCTA was chosen for HTL as a counterpart of ZnO ETL under the consideration of highest occupied molecular orbital (HOMO) energy level (5.7 eV)[23] close to VBM of InP@ZnSeS QDs (5.9 eV) and a hole mobility of $4 \times 10^{-4}$ cm$^2$ V$^{-1}$ s$^{-1}$ similar to the electron mobility of ZnO ETL.

Unlike the case of QLEDs with II−VI QDs, in which the electron injection takes place rather simultaneously even without applied voltage and the hole injection occurs under the assistance of electric field, the present QLEDs have a higher energetic barrier for electron injection from ZnO into InP@ZnSeS QDs (~0.5 eV) rather than the hole injection from TCTA into QDs (0.2 eV). The difference in the injection barrier for the electron and hole is likely to lead to asymmetric charge

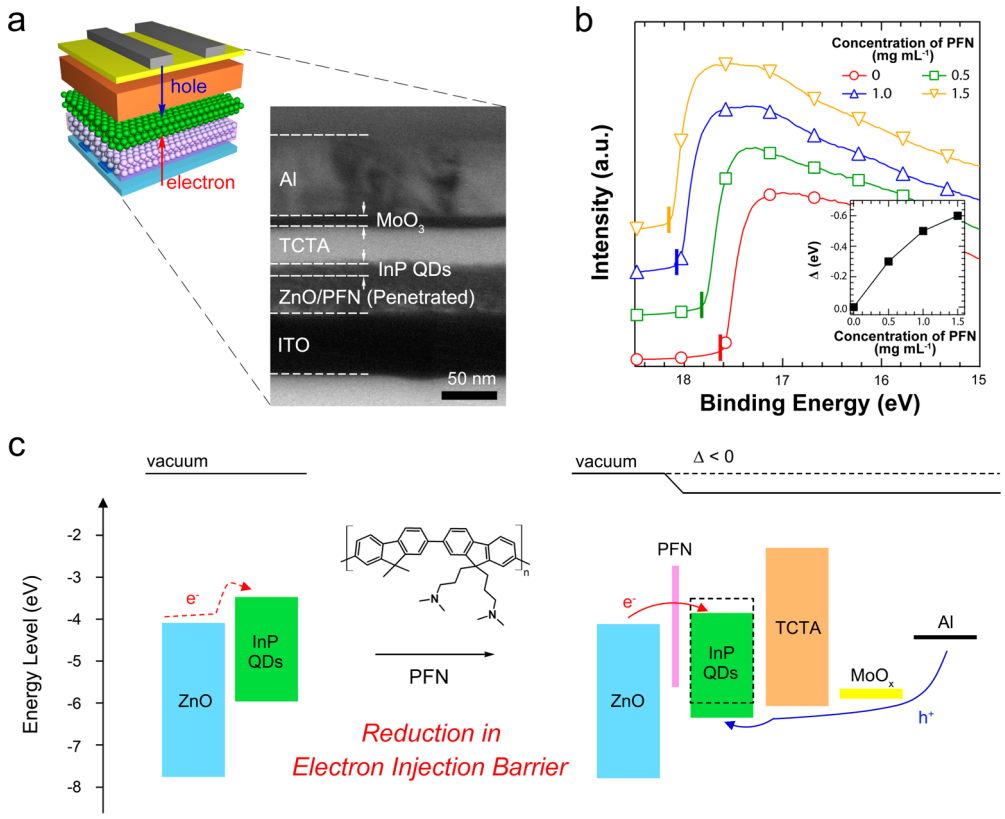


**Figure 2. (a) Schematic illustration (left) and a cross-sectional TEM image (right) of QLED in an inverted device structure. (b) Expanded UPS spectra near the binding energy cutoff region of a bare ZnO film and PFN-coated ZnO films on ITO substrates. The UPS spectra of PFN-coated ZnO films are vertically shifted for clarity. Inset: Change in the vacuum level shift (Δ) *vs* PFN concentration. (c) Flat band energy level diagrams of QLEDs illustrating the reduction in electron injection barrier between ZnO and QDs due to the presence of the PFN layer.**

injection and the charge imbalance within QDs (with excess of holes), which is responsible for the nonradiative exciton decay pathways *via* Auger recombination. In addition, such an injection barrier also increases the operational voltage (electric field) for QLEDs, which gives rise to the decrease in PL QY of QDs and subsequent operational efficiency loss in devices.[24]

A clear first step for the improvement in device performances is to facilitate the electron injection from ZnO into InP@ZnSeS QDs. From the aspect of the device structure, we have introduced a thin layer of poly-[(9,9-bis(3′-(*N*,*N*-dimethylamino)propyl)-2,7-fluorene)-*alt*-2,7-(9,9-ioctylfluorene)] (PFN) at the interface of ZnO with InP@ZnSeS QDs to reduce the electron injection barrier. The PFN, conjugated polyelectrolyte, serves as an interfacial dipole layer and is known to achieve a vacuum level shift over 0.5 eV.[25−28] In addition, PFN possesses poor solubility against nonpolar solvents (such as hexane or toluene) and enables orthogonal processing to realize multilayered structure (*i.e.*, ZnO nanocrystal layer/PFN thin layer/colloidal QD layer). On the basis of PFN, we could realign the carrier transport levels in the present QLEDs using the following architecture: on top of an ITO cathode, ZnO nanoparticle layer, PFN thin layer, and InP QD emission layer were sequentially spin-coated. TCTA, molybdenum oxide ($MoO_3$), and Al anode layers were then sequentially evaporated on top of the solution-processed ITO/ZnO/PFN/InP QD layer (Figure 2a).

The formation of an interfacial dipole layer and the corresponding vacuum level shift (Δ) at the interface of ZnO with InP@ZnSeS QDs were characterized with UPS spectra (Figure 2b). The extent of the vacuum level shift of the ITO/ZnO/PFN thin films could be adjusted up to 0.6 eV with the concentration of PFN solution (see the inset of Figure 2b). We note that the extent of the vacuum level shift saturates at 0.6 eV at a deposition with 1.5 mg $mL^{-1}$ of PFN concentration. Any significant change in surface morphology or roughness of ZnO ETLs was observed on PFN-covered ZnO films (Figure S2 and Table S3), which leads us to conclude that the difference in the device characteristics is essentially attributed to the changes in the electron injection properties between ZnO and InP@ZnSeS QDs *via* the vacuum level shift (Figure 2c) rather than the morphological changes in ZnO QDs or QD active layers.

To investigate the influence of the extent of the vacuum level shift on the electron injection characteristics, device performances were characterized as a function of PFN concentration (Figure 3). For systematic comparison, the other electronic components in QLEDs were optimized as 2−3 monolayers for

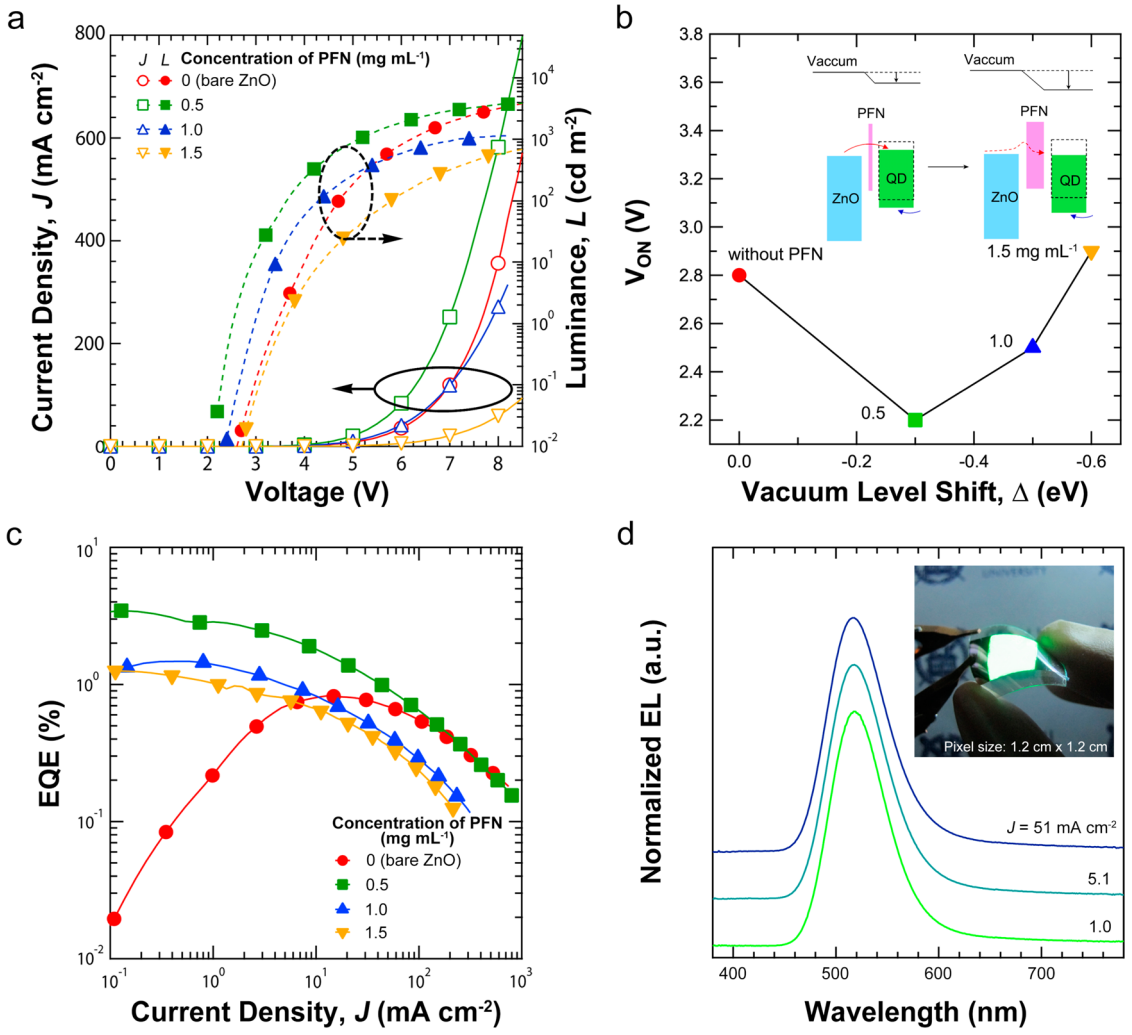


**Figure 3. (a) Current density−voltage−luminance ($J$−$V$−$L$) characteristics, (b) turn-on voltage ($V_{ON}$), and (c) EQE *vs* $J$ characteristics of InP@ZnSeS (1.7 nm shell thickness) QLEDs prepared with varied PFN concentrations. Vacuum level shift by PFN and corresponding arrangement of energy levels are illustrated as an inset in (b); the increase in the PFN thickness impedes electron tunneling from ZnO to QDs, thus $V_{OC}$ is increased again after optimal condition (green square). (d) Normalized EL spectra of InP@ZnSeS (1.7 nm shell thickness) QLEDs at different current densities ($J$). Inset: Photograph of large-area and flexible InP@ZnSeS QLED on a polyethersulfone substrate; pixel size = 1.2 cm × 1.2 cm.**

InP@ZnSeS QD emission layers (1.7 nm shell thickness), 40 nm for the ZnO nanoparticle layer, 50 nm for TCTA, and 10 nm for $MoO_x$. The presence of a thin PFN layer (0.5 mg $mL^{-1}$ of PFN) facilitated the electron injection from ZnO into InP@ZnSeS QDs, as evidenced by the significant decrease in the turn-on voltage ($V_{ON}$) from 2.8 to 2.2 V (Figure 3b) (which is close to the optical band gap) and the increase in $J$ and $L$ when compared with the reference device (without PFN) (Figure 3b). Interestingly, further increase in the PFN concentration did not guarantee improvement in device performances. Indeed, it resulted in a deleterious tendency in spite of the reduction in the electron injection barrier; the increase in PFN concentration above 0.5 mg $mL^{-1}$ led to the increased $V_{ON}$ as well as the decreased $J$ and $L$. This trade-off in device performances can be rationalized with the competing effects of PFN on charge injection from ZnO into QDs. A *thin* PFN layer acts as an interfacial dipole layer, reduces the potential difference between ZnO and InP@ZnSeS QDs *via* the vacuum level shift, and facilitates the electron injection from ZnO to QDs across the PFN layer (tunneling process). A *thick* PFN layer reduces the potential barriers further, but at the same time, expands the width of the tunneling barrier (the thickness of PFN itself) and thus impedes the tunneling of electrons from ZnO into the InP@ZnSeS QD emission layer. The summarized characteristics of QLEDs as a function of PFN deposition concentration are listed in Table 1.

The comprehensive adjustments of carrier transport layers facilitate the electron injection into InP QDs and consequently enhance the charge balance within QDs, as clearly evidenced by the dramatic increase in the device efficiency (Figure 3c). The optimized device with the thinnest PFN layer showed enhanced performance with 3.46% maximum EQE and 3900 cd $m^{-2}$ maximum

**TABLE 1. QLED Performance Based on Two Different QDs as a Function of PFN Concentration[a]**

| $t$ (nm) | PL QY (%) | EL $\lambda_{max}$/fwhm (nm) | PFN (mg mL$^{-1}$) | $V_{ON}$ (V) | max EQE (%) | EQE at 100 cd m$^{-2}$ (%) | max LE (cd A$^{-1}$) | max $L$ (cd m$^{-2}$) |
|---|---|---|---|---|---|---|---|---|
| 1.1 | 81 | 520/65 | 0.5 | 2.1 | 0.480 | 0.201 | 2.0 | 428 |
| 1.7 | 72 | 518/64 | 0 | 2.8 | 0.825 | 0.677 | 1.53 | 4182 |
| | | | 0.5 | 2.2 | 3.46 | 2.90 | 10.9 | 3900 |
| | | | 1 | 2.5 | 1.47 | 1.17 | 4.6 | 1138 |
| | | | 1.5 | 2.9 | 1.26 | 0.811 | 3.06 | 801 |

[a] Abbreviations and their full meanings: $t$ (shell thickness), PL QY (photoluminescence quantum yield of QDs), PL (photoluminescence), EL $\lambda_{max}$ (electroluminescence, at 1 mA/cm$^2$), $V_{ON}$ (turn-on voltage), EQE (external quantum efficiency), LE (luminous efficiency), and $L$ (luminance).

brightness without parasitic peaks from adjacent carrier transport layers under varied current densities (Figure 3d). Moreover, the large-area (1.2 cm × 1.2 cm) and flexible InP QLEDs with uniform brightness over the entire pixel could be demonstrated on the device platform (inset in Figure 3d), validating the process capability of PFN layers for practical applications toward large-area displays or lightings. To the best of our knowledge, the EQE, maximum brightness, and spectral purity of the present QLED devices record the highest values among Cd-free QD-based LEDs emitting visible light.

The direct injection of carriers and their charge balance are regarded as the key factors for efficient EL devices, which are clearly demonstrated in the current case. In the meantime, we found that the shell thickness of InP QDs is also responsible for the performance of InP QLEDs. On the basis of the optimized device structure, we compared the device performances of QLEDs employing InP@ZnSeS QDs with different shell thicknesses (1.1 and 1.7 nm). This comparison was possible by the advanced synthetic method presented above, preventing the formation of internal defect states in the shell phase while increasing the shell thickness (without the reduction in PL QY upon the increase in shell thickness due to lattice strain). It is surprising to note that InP@ZnSeS QDs with thicker shells clearly show better device performance in terms of EQE and maximum brightness than one with thinner shells (Figure S3 and Table 1).

Such distinct difference in EL efficiency of two QDs implies that the external conditions such as high electric field, large amount of charge carriers, or Joule heat are encountered during device operation. Considering the small CBM offset of InP@ZnSeS QDs and the light effective mass of the electron of InP, a high electric field could amplify the localization of electrons to the shell phase[29] (by pushing the electron cloud) or to surface states. The surface states have been known as a major origin of QD quenching, leading to the nonradiative exciton decay *via* the surface-state recombination or the Auger recombination activated by QD charging.[30−32]

*J*-dependent EL spectra of InP@ZnSeS QDs for different shell thickness provide intuitive clues to the contribution of extended ZnSeS shell phase on QLED

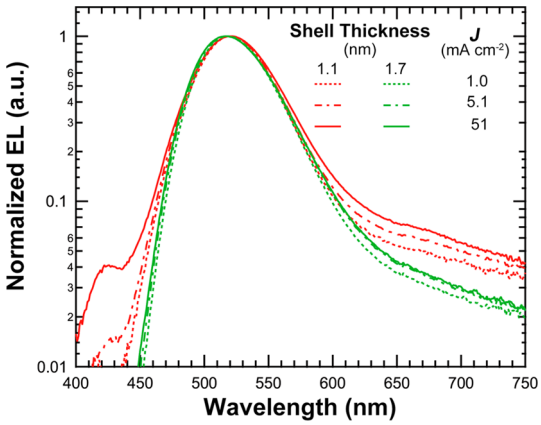


**Figure 4. Semilogarithmic normalized EL spectra of InP@ZnSeS QLEDs at different current densities: 1.1 nm (red) and 1.7 nm (green) shell thickness.**

performance. In the semilogarithmic plots of normalized EL spectra (Figure 4), two QLED devices based on two different types of QDs show faint emission tails (contribution to overall EL spectrum less than 10%), not detectable in solution PL. Interestingly, InP@ZnSeS QDs with 1.1 nm shell thickness show more distinct tails and increase with the increase in *J*. By contrast, InP@ZnSeS QDs with 1.7 nm shell thickness produce less significant tails which are almost independent of *J*. In general, broad emission below the optical band gap is known as a surface-state emission, originating from the carrier recombination occurring at surface states. Hence, the evolution of EL emission tails from InP@ZnSeS QDs with the thinner shell reflects the increased accessibility of electrically generated excitons to the surface states; under applied bias, the electric field drags electron wave functions outside and facilitates the surface-state-mediated recombination. At the same time, at high current density, a large amount of charge carriers can be trapped on surface states of QDs and increase the probability of surface-state emission, too.

In this context, we believe that the InP@ZnSeS QDs with 1.7 nm shell thickness buffer the delocalization of electrons from the inner part of the QDs by the electric field, resulting in the improved quantum efficiency of QLEDs. While the 1.1 nm shell thickness provides a marginal potential barrier and electrons are prone to access surface states, the increased shell thickness

provides sufficient potential barrier width against those processes. Interestingly, even an addition of 0.6 nm shell thickness resulted in the 7-fold enhancement in EQE, and it is attributed to an exponentially decreasing probability of electron wave functions in the potential barrier. Summing up, to minimize the surface-state-mediated exciton decay during device operation, we can conclude that the shell phase needs to be designed to possess the large band offset as well as the wide barrier width.

## CONCLUSIONS

In summary, we demonstrated environmentally benign, highly efficient, and bright InP@ZnSeS QLEDs based on the advanced synthetic method for InP QDs and the tailored device structures. From the practical point of view, the results given here certainly narrowed the gap between the device performance of Cd-free QLEDs and the industrial requirements for practical applications. The EQEs of InP QLEDs in the present study are the highest among other alternative technologies for Cd-free QLEDs available at the moment. More importantly, this could lead to important directions in terms of the structural design of devices and the core@shell formulation of QDs for further improvements of InP QLEDs. For the device structure, the proper choice and optimization of carrier transport materials were proven to be crucial for InP QLEDs to facilitate the direct injection of carriers. At the same time, we have shown that the thick ZnSeS heterostructured shell is important to increase EQEs of QLEDs, which protects electrically generated excitons from surface states. In a forthcoming study, we believe that deep investigation of nonradiative multicarrier decay during device operation and minute engineering in core@shell heterostructure minimizing such processes will guide us one step further toward high-performance InP QLEDs.

## EXPERIMENTAL METHODS

**Synthesis of InP@ZnSeS QDs.** Modified synthetic procedure by Lim *et al.* was adopted for the synthesis of InP@ZnSeS QDs.[18] Briefly, 0.1 mmol of $InCl_3$ in 1 mL of tetrahydrofuran, 2 mL of zinc oleate ($Zn(OA)_2$, 30 mmol of zinc acetate reacted with 19 mL of oleic acid (OA) under vacuum and diluted with 41 mL of 1-octadecene (ODE)), and 8 mL of ODE were loaded in a 100 mL flask with a condenser and degassed for 30 min to remove water and oxygen species. After backfilling the reactor with $N_2$, temperature was increased to 280 °C and a mixture of 0.1 mmol of $P(TMS)_3$ and 0.4 mmol of STBP (0.4 mmol of sulfur dissolved in 0.5 mL of TBP and 0.5 mL of ODE) was rapidly injected into the reactor. After 20 s, 0.2 mL of SeTOP (0.2 mmol of Se dissolved in 0.5 mL of *n*-trioctylphosphine and 0.5 mL of ODE) was slowly added for 20 s and reacted at 280 °C for 10 min. Next, 4 mL of $Zn(OA)_2$ and 1.8 mL of 1-dodecanethiol were added and reacted for 90 min at 300 °C. Finally, 6 mL of $Zn(OA)_2$ and 0.72 mL of 1-dodecanethiol were added, and the mixture was reacted for 120 min (for InP@ZnSeS QDs with 1.1 nm shell thickness, this step was omitted). After the reaction was terminated, the mixture was cooled to room temperature to terminate the reaction. For the purification of QDs, a precipitation/redispersion method was employed; the crude solution was precipitated with an excess amount of acetone and redispersed with toluene. After repeated purification processes (typically 4 times), the precipitated QDs were dried under $N_2$ flow for 5 min and dispersed in hexane (around 50 mg $mL^{-1}$).

**Photoluminescence Quantum Yield (PL QY) Measurement.** The PL QY was obtained by comparing their fluorescence intensities with the intensity of a primary standard dye solution (Coumarin 545, QY = 95% in ethanol) at the same excitation wavelength (400 nm). PL measurements were conducted on diluted solutions with absorbance below 0.05 at the excitation wavelength to minimize reabsorption between QDs. Specifically, the PL QY was calculated by the following equation:[33]

$$\text{PL QY} = 0.95 \times \frac{I_{QD}}{I_{dye}} \times \frac{A_{dye}}{A_{QD}} \times \frac{{n_{hexane}}^2}{{n_{ethanol}}^2} \quad (1)$$

In this equation, $I$ is the integrated area of a PL spectrum, $A$ is the absorbance of a solution at 400 nm, and $n$ is the refractive index of solvent used.

**Synthesis of ZnO Nanoparticles.** ZnO nanoparticles were synthesized modifying the method reported by Pacholski *et al.*[34] First, 3 g of zinc acetate dehydrate and 120 mL of methanol were placed in a three-neck round-bottom flask and heated to 60 °C. At that temperature, 60 mL of potassium hydroxide solution containing 1.51 g of KOH was injected dropwise into the zinc acetate dihydrate solution with strong agitation. The reaction mixture was kept at 60 °C for 2 h 15 min. At the end of the reaction, the product appeared as a milky solution. After being precipitated by centrifugation at 4000 rpm, the product was washed with methanol twice. Finally, the product was centrifuged again and redispersed in 5 mL of butanol.

**Determination of VBM and CBM of InP@ZnSeS QDs.** To estimate the energy levels of InP@ZnSeS QDs, a thin film of InP@ZnSeS QDs was fabricated on a ITO/ZnO substrate by spin-coating of 5 mg $mL^{-1}$ of a QD solution and dried under vacuum for 1 day. The UPS spectra were acquired using Kratos AXIS-NOVA, employing a He I light source and a hemispherical analyzer. A gold layer was introduced as a reference. The VBM position was determined by using the incident photon energy (21.2 eV), the high binding energy cutoff ($E_{cutoff}$), and the onset point in valence band region ($E_{onset}$) according to the equation below:

$$\text{VBM} = 21.2 - |E_{cutoff} - E_{onset}| \quad (2)$$

The CBM value was obtained by using the VBM and the excitonic band gaps of QDs, estimated from the PL spectra of QDs. UPS spectra of two different InP@ZnSeS QDs and optical band gap are provided in the Supporting Information.

**Device Fabrication and Characterization.** InP QLEDs were fabricated on patterned ITO glass substrates, cleaned with isopropyl alcohol, acetone, and methanol in an ultrasonic bath. First, 30 mg $mL^{-1}$ of a ZnO solution was spun on a patterned ITO substrate at 2000 rpm for 60 s and baked in $N_2$ atmosphere at 90 °C for 30 min. The resulting film thickness was 45 nm. Then, 0.5 mg $mL^{-1}$ of PFN (purchased from 1-materials Inc.) solution in methanol/acetic acid solution (methanol/acetic acid = 2 $\mu$L/1 mL) was spun on the ZnO layer and dried for 30 min under vacuum. Then, a 5 mg $mL^{-1}$ QD dispersion was deposited by spin-casting at 4000 rpm for 30 s, equivalent to the 2−3 monolayers of QDs. Finally, TCTA (50 nm), $MoO_3$ (10 nm), and Al (100 nm) were sequentially evaporated with a deposition rate of 0.5−1, 0.2, and 3−5 Å $s^{-1}$, respectively. The current−voltage−luminance characteristics were measured using a Keithley 236 source measure unit and a Keithley 2000 multimeter coupled with a calibrated Si photodiode. Electroluminescence spectra of QLEDs prepared in the present study were obtained using a Konica-Minolta CS-1000A spectroradiometer.

*Conflict of Interest:* The authors declare no competing financial interest.

*Acknowledgment.* This work was financially supported by the National Research Foundation of Korea (NRF) grant funded by the Korea government Ministry of Science, ICT & Future Planning (MSIP): the National Creative Research Initiative Center for Intelligent Hybrids (No. 2010-0018290), the WCU Program of C2E2 (R31-10013), the Technology Development Program to Solve Climate Changes (No. NRF-2009-C1AAA001-2009-0093282), and the Brain Korea 21 Program. This work was also supported by the Industrial Strategic Technology Development Program (10045145, development of high performance (>70 $cm^2$/Vs) chalcogenide TFT backplane and cadmium-free highly efficient (>30 cd/A) hybrid EL material/devices) funded by the Ministry of Trade, Industry and Energy (MOTIE, Korea).

*Supporting Information Available:* Atomic composition of InP QDs, device fabrication, and their characterization. This material is available free of charge *via* the Internet at http://pubs.acs.org.

## REFERENCES AND NOTES


1. Lim, J.; Bae, W. K.; Kwak, J.; Lee, S.; Lee, C.; Char, K. Perspective on Synthesis, Device Structures, and Printing Processes for Quantum Dot Displays. *Opt. Mater. Express* **2012**, *2*, 594–628.
2. Bae, W. K.; Char, K.; Hur, H.; Lee, S. Single-Step Synthesis of Quantum Dots with Chemical Composition Gradients. *Chem. Mater.* **2008**, *20*, 531–539.
3. Bae, W. K.; Nam, M. K.; Char, K.; Lee, S. Gram-Scale One-Pot Synthesis of Highly Luminescent Blue Emitting $Cd_{1-x}Zn_xS$/ZnS Nanocrystals. *Chem. Mater.* **2008**, *20*, 5307–5313.
4. Kim, S.; Kim, T.; Kang, M.; Kwak, S. K.; Yoo, T. W.; Park, L. S.; Yang, I.; Hwang, S.; Lee, J. E.; Kim, S. K.; *et al.* Highly Luminescent InP/GaP/ZnS Nanocrystals and Their Application to White Light-Emitting Diodes. *J. Am. Chem. Soc.* **2012**, *134*, 3804–3809.
5. Li, L.; Reiss, P. One-Pot Synthesis of Highly Luminescent InP/ZnS Nanocrystals without Precursor Injection. *J. Am. Chem. Soc.* **2008**, *130*, 11588–11589.
6. Talapin, D. V.; Mekis, I.; Götzinger, S.; Kornowski, A.; Benson, O.; Weller, H. CdSe/CdS/ZnS and CdSe/ZnSe/ZnS Core–Shell–Shell Nanocrystals. *J. Phys. Chem. B* **2004**, *108*, 18826–18831.
7. Xie, R.; Kolb, U.; Li, J.; Basché, T.; Mews, A. Synthesis and Characterization of Highly Luminescent CdSe–Core CdS/$Zn_{0.5}Cd_{0.5}S$/ZnS Multishell Nanocrystals. *J. Am. Chem. Soc.* **2005**, *127*, 7480–7488.
8. Mashford, B. S.; Stevenson, M.; Popovic, Z.; Hamilton, C.; Zhou, Z.; Breen, C.; Steckel, J.; Bulovic, V.; Bawendi, M.; Coe-Sullivan, S.; *et al.* High-Efficiency Quantum-Dot Light-Emitting Devices with Enhanced Charge Injection. *Nat. Photonics* **2013**, *7*, 407–412.
9. Rizzo, A.; Mazzeo, M.; Biasiucci, M.; Cingolani, R.; Gigli, G. White Electroluminescence from a Microcontact-Printing-Deposited CdSe/ZnS Colloidal Quantum-Dot Monolayer. *Small* **2008**, *4*, 2143–2147.
10. Kim, L.; Anikeeva, P. O.; Coe-Sullivan, S. A.; Steckel, J. S.; Bawendi, M. G.; Bulović, V. Contact Printing of Quantum Dot Light-Emitting Devices. *Nano Lett.* **2008**, *8*, 4513–4517.
11. Kim, T.-H.; Cho, K.-S.; Lee, E. K.; Lee, S. J.; Chae, J.; Kim, J. W.; Kim, D. H.; Kwon, J.-Y.; Amaratunga, G.; Lee, S. Y.; *et al.* Full-Colour Quantum Dot Displays Fabricated by Transfer Printing. *Nat. Photonics* **2011**, *5*, 176–182.
12. Haverinen, H. M.; Myllyla, R. A.; Jabbour, G. E. Inkjet Printing of Light Emitting Quantum Dots. *Appl. Phys. Lett.* **2009**, *94*, 073108-3.
13. Singh, M.; Haverinen, H. M.; Dhagat, P.; Jabbour, G. E. Inkjet Printing—Process and Its Applications. *Adv. Mater.* **2010**, *22*, 673–685.
14. Kazlas, P. T.; Zhou, Z.; Stevenson, M.; Niu, Y.; Breen, C.; Kim, S.-J.; Stecket, J. S.; Coe-Sullivan, S.; Ritter, J. 32.4: Quantum Dot Light Emitting Diodes for Full-Color Active-Matrix Displays. *Dig. Tech. Pap. — Soc. Inf. Disp. Int. Symp* **2010**, *41*, 473–476.
15. Yang, X.; Divayana, Y.; Zhao, D.; Leck, K. S.; Lu, F.; Tan, S. T.; Abiyasa, A. P.; Zhao, Y.; Demir, H. V.; Sun, X. W. A Bright Cadmium-Free, Hybrid Organic/Quantum Dot White Light-Emitting Diode. *Appl. Phys. Lett.* **2012**, *101*, 233110.
16. Maier-Flaig, F.; Rinck, J.; Stephan, M.; Bocksrocker, T.; Bruns, M.; Kübel, C.; Powell, A. K.; Ozin, G. A.; Lemmer, U. Multicolor Silicon Light-Emitting Diodes (SiLEDs). *Nano Lett.* **2013**, *13*, 475–480.
17. Chen, B.; Zhong, H.; Zhang, W.; Tan, Z. A.; Li, Y.; Yu, C.; Zhai, T.; Bando, Y.; Yang, S.; Zou, B. Highly Emissive and Color-Tunable $CuInS_2$-Based Colloidal Semiconductor Nanocrystals: Off-Stoichiometry Effects and Improved Electroluminescence Performance. *Adv. Funct. Mater.* **2012**, *22*, 2081–2088.
18. Lim, J.; Bae, W. K.; Lee, D.; Nam, M. K.; Jung, J.; Lee, C.; Char, K.; Lee, S. InP@ZnSeS, Core@Composition Gradient Shell Quantum Dots with Enhanced Stability. *Chem. Mater.* **2011**, *23*, 4459–4463.
19. Ippen, C.; Greco, T.; Wedel, A. InP/ZnSe/ZnS: A Novel Multishell System for InP Quantum Dots for Improved Luminescence Efficiency and Its Application in a Light-Emitting Device. *J. Inf. Disp.* **2012**, *13*, 91–95.
20. Mahler, B.; Spinicelli, P.; Buil, S.; Quelin, X.; Hermier, J.-P.; Dubertret, B. Towards Non-blinking Colloidal Quantum Dots. *Nat. Mater.* **2008**, *7*, 659–664.
21. García-Santamaría, F.; Chen, Y.; Vela, J.; Schaller, R. D.; Hollingsworth, J. A.; Klimov, V. I. Suppressed Auger Recombination in "Giant" Nanocrystals Boosts Optical Gain Performance. *Nano Lett.* **2009**, *9*, 3482–3488.
22. Bae, W. K.; Padilha, L. A.; Park, Y.-S.; McDaniel, H.; Robel, I.; Pietryga, J. M.; Klimov, V. I. Controlled Alloying of the Core–Shell Interface in CdSe/CdS Quantum Dots for Suppression of Auger Recombination. *ACS Nano* **2013**, *7*, 3411–3419.
23. Kwak, J.; Bae, W. K.; Lee, D.; Park, I.; Lim, J.; Park, M.; Cho, H.; Woo, H.; Yoon, D. Y.; Char, K.; *et al.* Bright and Efficient Full-Color Colloidal Quantum Dot Light-Emitting Diodes Using an Inverted Device Structure. *Nano Lett.* **2012**, *12*, 2362–2366.
24. Shirasaki, Y.; Supran, G. J.; Tisdale, W. A.; Bulović, V. Origin of Efficiency Roll-Off in Colloidal Quantum-Dot Light-Emitting Diodes. *Phys. Rev. Lett.* **2013**, *110*, 217403.
25. Huang, F.; Wu, H.; Wang, D.; Yang, W.; Cao, Y. Novel Electroluminescent Conjugated Polyelectrolytes Based on Polyfluorene. *Chem. Mater.* **2004**, *16*, 708–716.
26. Wu, H.; Huang, F.; Mo, Y.; Yang, W.; Wang, D.; Peng, J.; Cao, Y. Efficient Electron Injection from a Bilayer Cathode Consisting of Aluminum and Alcohol-/Water-Soluble Conjugated Polymers. *Adv. Mater.* **2004**, *16*, 1826–1830.
27. Wu, H.; Huang, F.; Peng, J.; Cao, Y. High-Efficiency Electron Injection Cathode of Au for Polymer Light-Emitting Devices. *Org. Electron.* **2005**, *6*, 118–128.
28. Guan, X.; Zhang, K.; Huang, F.; Bazan, G. C.; Cao, Y. Amino N-Oxide Functionalized Conjugated Polymers and Their Amino-Functionalized Precursors: New Cathode Interlayers for High-Performance Optoelectronic Devices. *Adv. Funct. Mater.* **2012**, *22*, 2846–2854.
29. Bozyigit, D.; Yarema, O.; Wood, V. Origins of Low Quantum Efficiencies in Quantum Dot LEDs. *Adv. Funct. Mater.* **2013**, *23*, 3024–3029.
30. Klimov, V. I.; Mikhailovsky, A. A.; McBranch, D. W.; Leatherdale, C. A.; Bawendi, M. G. Quantization of Multiparticle Auger Rates in Semiconductor Quantum Dots. *Science* **2000**, *287*, 1011–1013.
31. Solov'ev, I. Y.; Zegrya, G. G. Nonradiative Recombination in Quantum Dots *via* Coulomb Interaction with Carriers in the Barrier Region. *Appl. Phys. Lett.* **2003**, *82*, 2571–2573.
32. Robel, I.; Gresback, R.; Kortshagen, U.; Schaller, R. D.; Klimov, V. I. Universal Size-Dependent Trend in Auger Recombination in Direct-Gap and Indirect-Gap Semiconductor Nanocrystals. *Phys. Rev. Lett.* **2009**, *102*, 177404.
33. Crosby, G. A.; Demas, J. N. Measurement of Photoluminescence Quantum Yields. Review. *J. Phys. Chem.* **1971**, *75*, 991–1024.
34. Pacholski, C.; Kornowski, A.; Weller, H. Self-Assembly of ZnO: From Nanodots to Nanorods. *Angew. Chem., Int. Ed.* **2002**, *41*, 1188–1191.